Madencilik - Mining, 2024, 63(2), 101-110

BİLİMSEL MADENCİLİK DERGİSİ
SCIENTIFIC MINING JOURNAL

TMMOB Maden Mühendisleri Odası Yayını / The Publication of the Chamber of Mining Engineers of Turkey

www.mining.org.tr

Research Article

Reasonable width of coal pillar in fully mechanized caving mining face of extra-thick coal seam–A case study

Xueqi Zhang[1, 2, *], Hongbin Li[1,**], Yongwei Du[1,***], Zhongqiu Wang[1,****]

1 Inner Mongolia Yitai Coal Co., Ltd., Ordos, Inner Mongolia, 017000, China
2 State Key Laboratory of Coal Mine Disaster Dynamics and Control, Chongqing University, Chongqing, 400044, China

Received: 30 December 2024 • Accepted: 26 March 2025

A B S T R A C T

To address the issue of resource wastage caused by the extraction of thick coal seams with large coal pillars, this study is based on the first Panel of the 110 Working Face at the Suancigou Coal Mine. It employs methods such as on-site measurement, physical similarity model experiments, theoretical analysis, and numerical simulation to investigate the reasonable width of coal pillars under the disturbance of comprehensive mechanized mining in thick coal seams. The study reveals the damage and deformation evolution patterns of the coal pillars, calculates the critical width of the coal pillars based on limit equilibrium theory and strength theory, and simulates the distribution characteristics of stress and damage failure zones in the coal pillars. The results indicate that a 45 m coal pillar still possesses the substantial load-bearing capacity after multiple mining activities, suggesting the possibility of reducing its width to enhance coal recovery rates. The calculations show that the minimum width of the coal pillar should not be less than 26.18 m. Simulations demonstrate that when the width of the coal pillar is 30 m, the coal recovery rate is relatively high and meets safety production requirements. The findings of this research are significant for improving coal recovery rates in the Suancigou Coal Mine and similar mining conditions.

Keywords: *damage and deformation evolution; critical width; stress distribution; reasonable width; damage and failure zone.*

Introduction

Coal accounts for 60-70% of China's primary energy consumption structure and serves as the fundamental guarantee of energy security (Xie et al., 2021; Chen et al., 2021). Among them, the extra-thick coal seam is the main coal seam with high productivity and high efficiency, which is distributed in all major mining areas in China. Extra-thick coal seams are generally mined by longwall fully mechanized top coal caving, and a certain width of coal pillar is usually reserved between adjacent working faces to ensure the stability of the roadway. Therefore, the setting of the coal pillar width is crucial (Yuan et al., 2023). If the coal pillar is too narrow, it is prone to instability and failure, making it difficult to control the roadway; if it is too wide, it may lead to issues such as low coal recovery rates (Yang et al., 2022; He et al., 2023; Xue et al., 2024; Liu et al., 2023).

The most widely used method at present is A.H. Wilson's coal pillar design theory and formula, which overcomes the shortcomings of other methods, making it more practical and reliable (Gao et al., 2022). However, in actual applications, simplified empirical formulas are used, which only consider the coal pillar's ultimate strength and the width of the yielding zone (Yin et al., 2022; Song, 2016; Chen, 2005; Guo et al., 2014). With the introduction of long-term strength parameters of coal, the issue of insufficient consideration of coal pillar long-term strength in the theory has been addressed (Wang et al., 2002). Today, the application of advanced reasonable coal pillar design theories and methods, such as numerical simulation (Chang and Xu, 2021; Tian et al., 2021), internal and external stress field theories (Zheng et al., 2019; Li et al., 2012), and limit equilibrium theory coupled with elastoplastic theory (Kong et al., 2022; Wang and Dou, 2022; Zhu et al., 2021), has led to the continuous rationalization of coal pillar width design. However, in some long-operating mines, the coal pillar width design still relies on single or outdated theoretical methods. To ensure mining safety (Xing et al., 2024; Gu et al., 2024; Li et al., 2023), designs are overly conservative, leading to excessively large coal pillar widths, which result in significant coal resource wastage. Therefore, it is urgent to conduct relevant research, optimize coal pillar widths, and improve coal recovery rates.

To address the above-mentioned issues, this study took the 6_{upper}110 Working Face in the First Panel of Suancigou Coal Mine as the research background. Methods such as on-site monitoring, theoretical analysis, and numerical simulation were employed to study the reasonable width of the original 45-meter coal pillar.

* Corresponding author: qzhang1980@163.com • https://orcid.org/0009-0009-5491-9550
** lihb@mail.vinhelp.com • https://orcid.org/0009-0004-1668-5080
*** yidu195880698@163.com • https://orcid.org/0009-0001-4995-1515
**** zhongxunwang231@sina.com • https://orcid.org/0009-0000-0676-9652

https://DOI: 10.30797/madencilik.1609775

The study analyzed the damage and deformation evolution of the coal pillar, calculated the critical width of the coal pillar based on limit equilibrium theory and strength theory, and simulated the distribution characteristics of the coal pillar's stress and damage failure zones (Rong et al., 2024; Li et al., 2024; Liu et al., 2024; Yun et al., 2024). The research findings solved the problem of significant coal resource wastage caused by excessively large coal pillar widths at Suancigou Coal Mine. Additionally, the results provided a reference for optimizing coal pillar design in similar mining conditions.

1. Engineering background

1.1 Project Overview

The Suancigou Coal Mine is in the central region of the Jungar Coalfield in Inner Mongolia. It was completed and began trial production in August 2008. The mine covers an area of 49.82 km^2, with a reserve of 136,690,000 tons and an annual production capacity of 18 million tons. Currently, the mine primarily extracts from the 6_{upper} coal seam, which has a thickness ranging from 8 to 30 meters, with an average thickness of 20 meters. The immediate roof consists of medium sandstone with an average thickness of 22.2 meters, and the main roof is made up of sandy mudstone with an average thickness of 4.2 meters. The 110 Working Face is an active mining face, located in the northern wing of the First Panel in the northeastern part of the mine. The face has an approximately northeast-southwest orientation, with a strike length of 2,058 meters and a dip width of 244.6 meters. The area of the working face is 503,387 m^2, with a designed mining height of 3.8 meters and a maximum mining height of 24.2 meters, resulting in a mining ratio of 1:6. The layout of the roadways is shown in Figure 1.

1.2 Mine Pressure Manifestation Characteristics of Roadways and Stress Variation Patterns of Coal Pillars

(1) Deformation and Stress Characteristics of Roadways

Monitoring stations are set up in the 108 Transportation roadway, as shown in Figure 1, where the mine pressure manifestation characteristics are observed during the recovery of the 110 Working Face.

① Surface displacement analysis of the surrounding rock in the 108 Transportation Roadway (Figure 2)

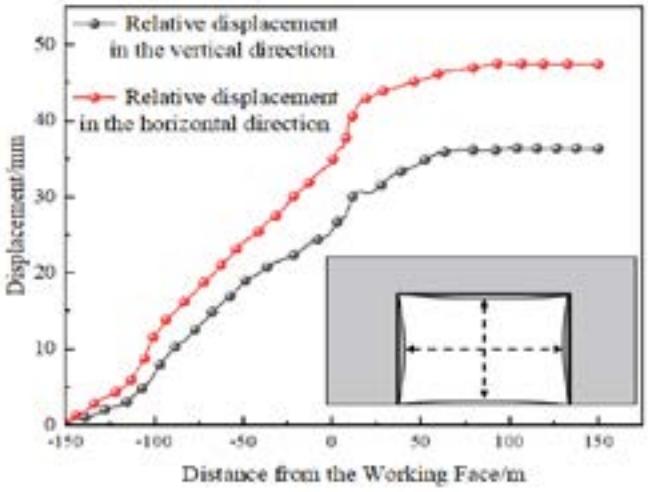

Fig.2 Evolutionary law of roadway surface displacement with advancement of working face

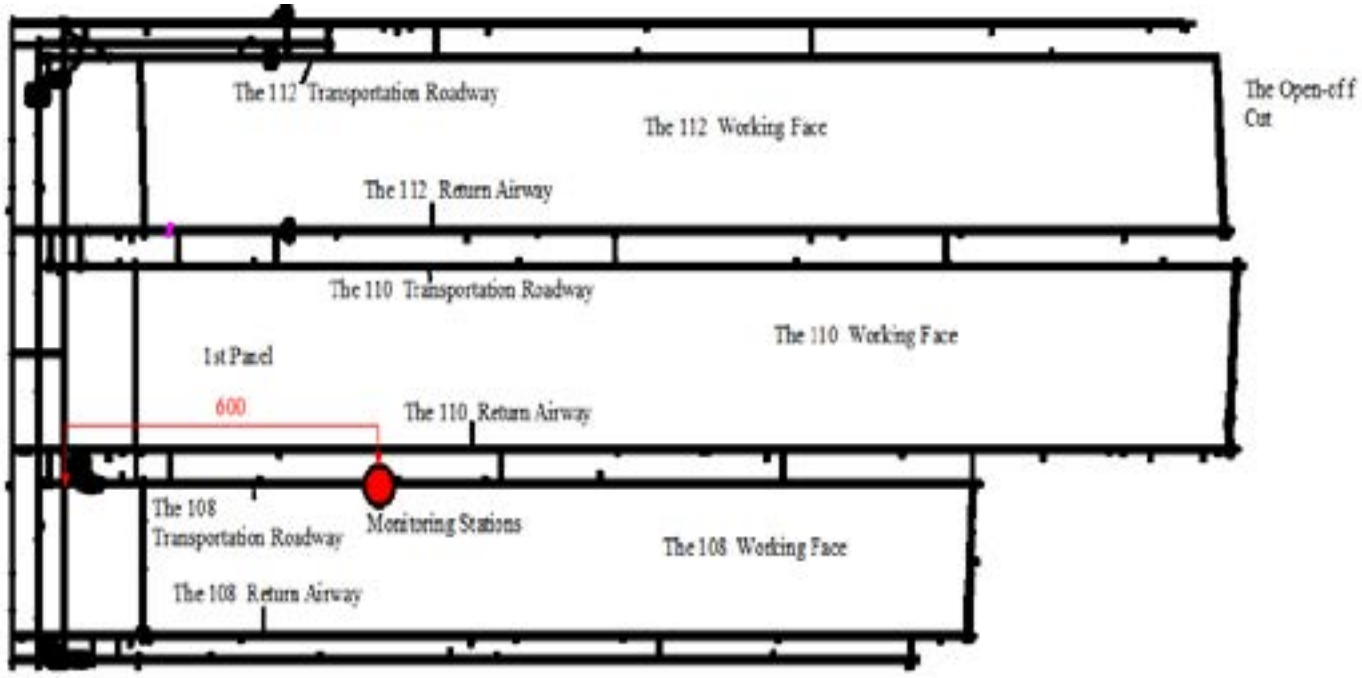

Fig.1 The layout of the roadways

During the observation period, the relative convergence of the surrounding rock in the 108 Transportation Roadway at the roof-floor and left-right sides is 48 mm and 37 mm, respectively. The surface deformation velocity of the surrounding rock in the range of -110 to 70 meters from the working face is relatively high, with the maximum relative displacement velocities of the roof-floor and left-right sides reaching 4 mm/s and 3 mm/s, respectively. As the working face advances, the surface deformation velocity of the surrounding rock in the 108 Transportation Roadway continuously decreases. After reaching 60 meters from the working face, the deformation velocity of the surrounding rock tends to stabilize, and the deformation of the roadway surrounding rock also becomes stable.

② Roof Stratum Separation Analysis of the 108 Transportation Roadway (Figure 3)

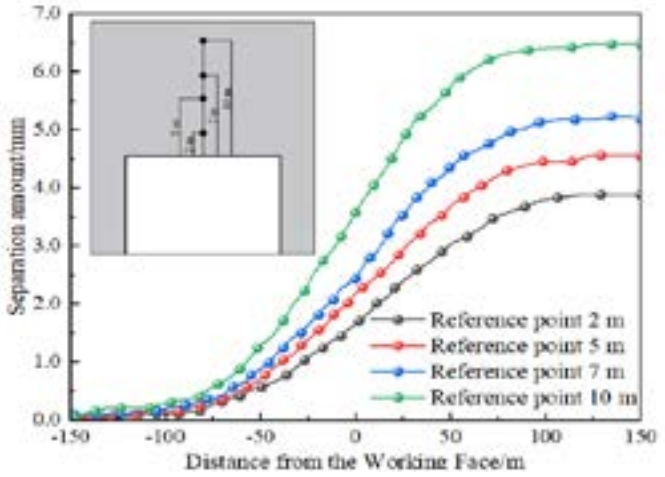

Fig.3 Variation law of roof stratum separation with the advancement of the working face

From Figure 3, the roof stratum separation in the 108 Transportation roadway mainly occurs between 80 meters ahead and 65 meters behind the 110 Working Face. Overall, as the reference point depth increases, the separation amount also increases. The maximum separation occurs at a depth of 10 meters in the roof, but the maximum separation is only 3.25 mm, indicating that roof separation is not significant. Based on the monitoring results of roof stratum separation in the 108 Transportation Roadway, it can be concluded that the recovery of the 110 Working face has little impact on the roof separation in the 108 Transportation Roadway. It is analyzed that the 45-meter protective coal pillar effectively ensures the stability of the 108 Transportation Roadway and limits the occurrence of significant roof separation.

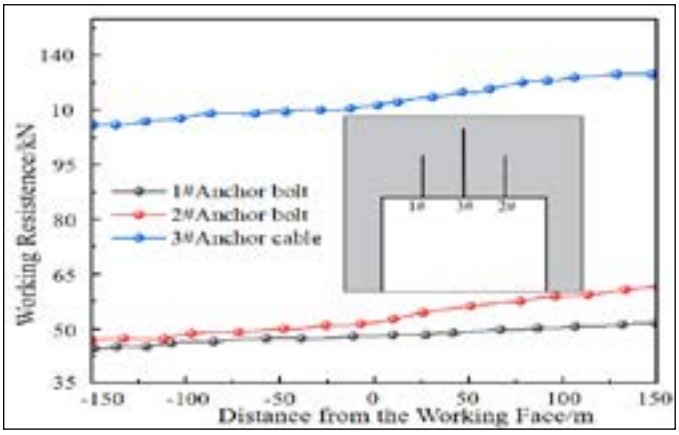

Fig.4 Variation law of anchor bolt(cable) working resistance with the advancement of the working face

From Figure 4, it can be observed that the working resistance of anchor bolts (cables) in the 108 Transportation Roadway shows minimal changes during the recovery of the 110 Working Face, generally tending towards a stable state. Within the monitoring range of 150 meters ahead and behind, the working resistance of anchor bolts (cables) in the 108 Transportation Roadway exhibits a slow increasing trend: the 1# anchor bolt increases by 6.9 kN, the 2# anchor cable increases by 14.4 kN, and the 3# anchor cable increases by 14 kN.

The roadway pressure monitoring results indicate that during the recovery of the 110 Working Face, the surface displacement and roof separation in the 108 Transportation Roadway are relatively small, and the working resistance of the anchor bolts (cables) shows minimal variation, reflecting good roadway system stability. The analysis suggests that the 45-meter coal pillar is the key factor ensuring the stability of the 108 Transportation Roadway system. The large width of the protective coal pillar minimizes the impact of mining activities on the exposed roadway, resulting in insignificant roadway pressure manifestation.

(2) Stress Variation Law of Coal Pillars

A group of borehole stress meters is installed at the same position as the roadway pressure monitoring station, as shown in Figure 2, to monitor the stress distribution law of the protective coal pillar within the range of 150 meters ahead to 150 meters behind the 110 Working Face. The monitoring results are shown in Figure 5. It should be noted that the results in the figure represent the stress increment caused by production activities at the working face, with the stress increment set to zero at 150 meters ahead of the working face (i.e., -150 m).

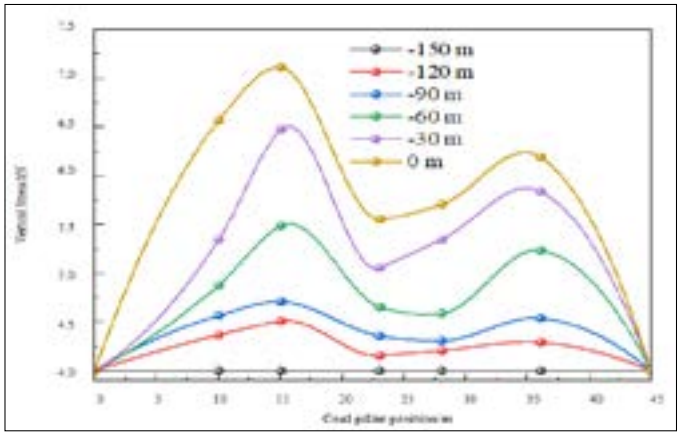

(a) From -150 m to 0 m relative to the working face

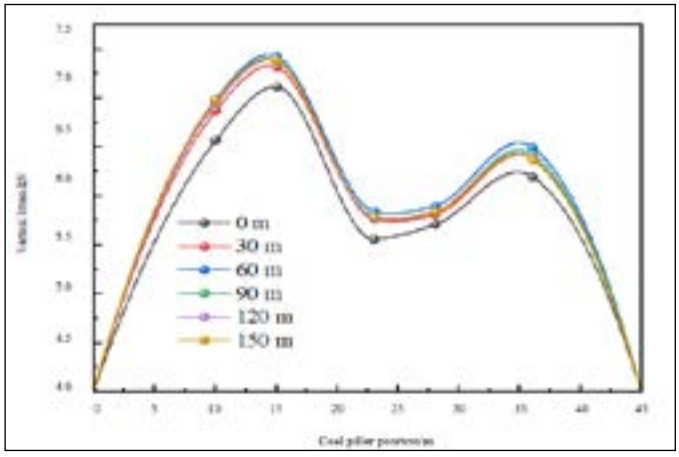

(b) From 0 m to 150 m relative to the working face

Fig.5 Variation law of coal pillar stress increment with the advancement of the working face

From Figure 5, it can be observed that under the influence of single-sided mining activity at the 110 Working Face, the stress increment of the coal pillar exhibits a double-peak asymmetric distribution pattern, with a greater increase in stress on the coal pillar near the goaf. As the 110 Working Face advances, the distance between the monitoring station and the working face gradually decreases, causing the load from the roof strata to transfer to the coal seam, which gradually increases the pressure on the coal pillar and leads to a continuous rise in the stress increment. The maximum stress increment occurs at 15 meters from the 110 Working Face, as shown in Figure 5(a). After the 110 Working Face advances a certain distance past the monitoring point, the stress increment of the coal pillar shows a negative growth trend, as illustrated in Figure 5(b). This is analyzed to be due to a slight release or transfer of coal pillar stress following periodic fracture of the roof strata. As the working face advances further, the stress increment of the coal pillar stabilizes, indicating that the stress distribution of the coal pillar gradually stabilizes.

Under the influence of mining activities at the 110 Working Face, the coal pillar near the goaf gradually fails, with the yielding failure region expanding inward and its load-bearing capacity gradually decreasing. However, due to the large width of the coal pillar, the coal pillar on the side of the 108 Working Face is less affected by mining activities over a larger area and still retains a high load-bearing capacity, maintaining a significant proportion of its elastic region. Therefore, based on the roadway pressure monitoring results of the 108 Transport Roadway, it is concluded that the original coal pillar width can be appropriately reduced to some extent to improve the coal resource recovery rate of the mine.

2. Characteristics of Coal Pillar Failure

The failure characteristics of the coal pillar are analyzed by combining a two-dimensional physical similarity model test with field measurements, based on the overburden distribution and its physical and mechanical characteristics in the Suancigou Coal Mine (Yang et al., 2023; Cao and Wei, 2024; Yang et al., 2024).

Table 1 Basic parameters of the physical similarity model

Item	Parameter	Item	Parameter
Model Length	2.6 m	Excavation Distance	2.2 m
Model Thickness	0.3 m	Model Boundary	10 cm
Model Height	1.54 m	Excavation Steps	44
Coal Seam Thickness	10 cm	Excavation Distance per Step	5 cm
Geometric Ratio	200:1	Excavation Time Interval	0.5 h
Density Ratio	1:1	Excavation Time	22 h
Stress Ratio	200:1	Upper Load	0.0355 MPa

The experiment is conducted using a similar simulation test platform at the State Key Laboratory of Coal Mine Disaster Dynamics and Control of Chongqing University. The geometric similarity ratio C_1 of the model is 1:200. The basic parameters of the model are shown in Table 1, and the physical model is shown in Figure 6.

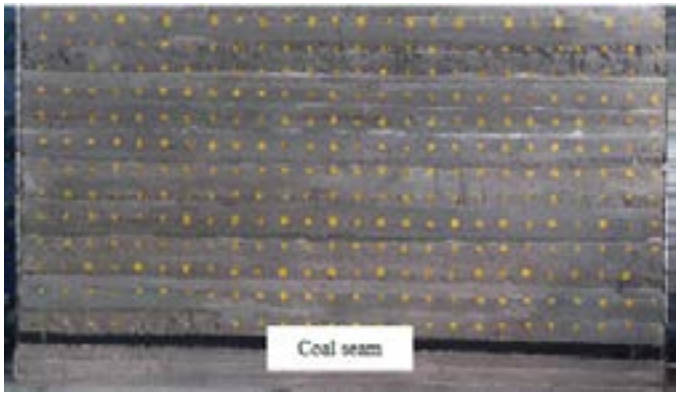

Fig.6 Physical similarity model

2.1 Analysis of Experimental Results

Figure 7 shows the deformation and damage characteristics of the coal pillar after excavation on both sides of the working face.

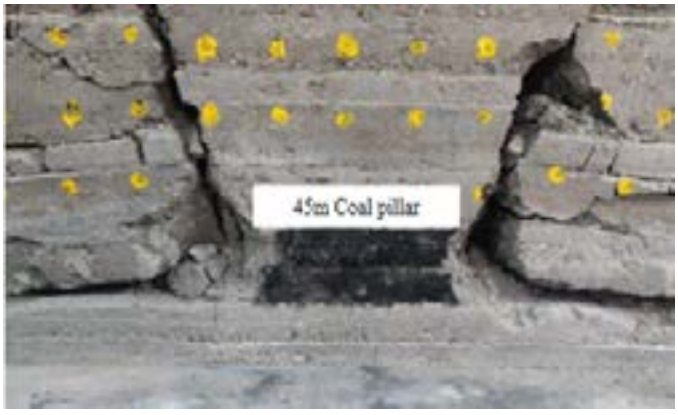

Fig.7 The deformation characteristics of the coal pillar

From Figure 7, it can be concluded that the influence of mining-induced stress from the left-side working face causes a certain amount of block collapse on the coal pillar near the goaf, accompanied by the formation of fractures. As the right-side working face is mined, the damage degree of the coal pillar on the goaf side of the left-side working face further intensifies, with an increased amount of block collapse and more extensive fracture development. Similar phenomena also occur in the coal pillar near the goaf of the right-side working face.

Overall, the damage caused by mining-induced stress to the coal pillar occurs only on both sides of the coal pillar, with minimal impact on its elastic core zone. After mining on both the left and right working faces, a relatively wide elastic zone still exists within the coal pillar, maintaining a high load-bearing capacity.

Therefore, to improve the coal recovery rate of the 6th Upper coal seam at Suancigou Coal Mine, the width of the coal pillar between working faces can be appropriately reduced, which will effectively enhance the coal resource recovery rate.

2.2 Evolution Characteristics of Coal Pillar Damage and Deformation

Based on the results of field monitoring and physical similarity simulation tests, the evolution characteristics of damage and deformation in the protective coal pillars of the First Panel working face at Suancigou Coal Mine are obtained, as shown in Figure 8.

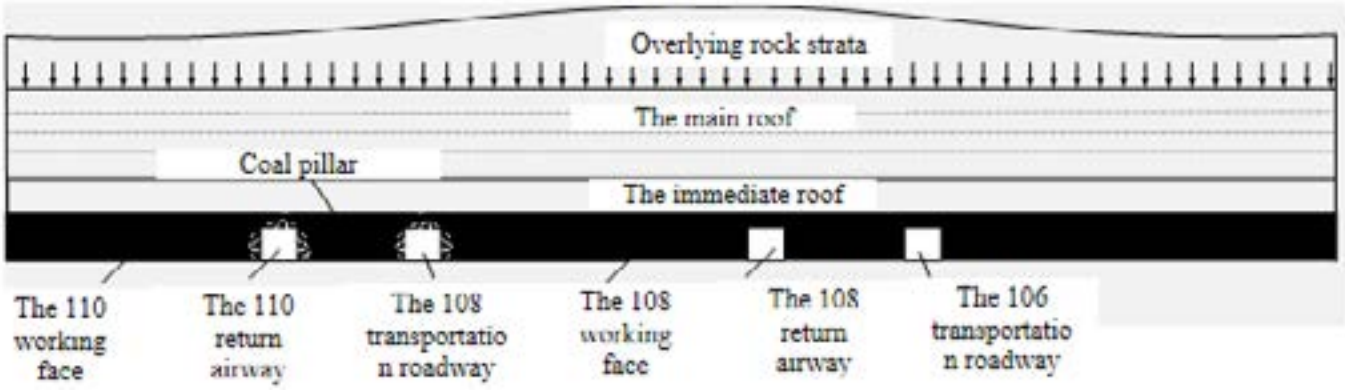

(a) Phase 1: Roadway Excavation

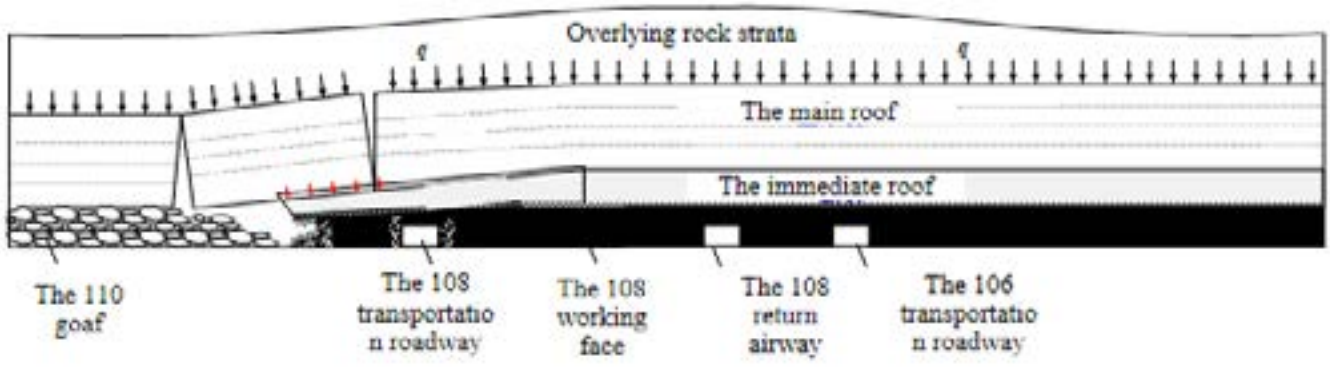

(b) Phase 2: Recovery of the 6th 110 Working Face

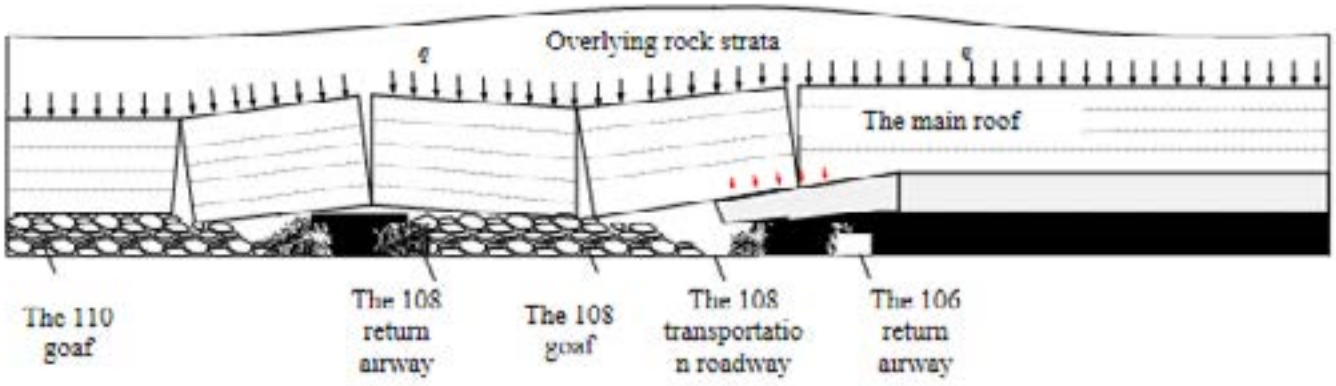

(c) Phase 3: Recovery of the 6_{upper} 108 Working Face

Fig.8 Coal pillar deformation characteristics

From Figure 8, it can be seen that the deformation and damage of the coal pillar can be divided into three stages:

① Phase 1: This is the stage where the coal pillar is influenced by roadway excavation for the recovery of the 110 Working Face and the 108 Working Face. During this phase, a loosened zone of approximately 1-2 meters is formed in the coal pillar, as shown in Figure 8(a).

② Phase 2: This is the stage where the coal pillar is influenced by the first mining activity at the 110 Working Face. During this phase, slight separations occur on the side of the coal pillar near the 108 Working Face within the 45-meter pillar between the 110 Return Airway and the 108 Transport Roadway. The elastic zone in the middle of the coal pillar decreases, forming stress concentration areas. The stress peak and the plastic zone gradually expand toward the deeper regions of the coal pillar, reducing its load-bearing capacity. A larger plastic zone is formed on the side of the coal pillar near the 110 Working Face, as shown in Figure 8(b).

③ Phase 3: This is the stage where the coal pillar is influenced by the second mining activity at the 108 Working Face. During this phase, separations occur on both sides of the 45-meter coal pillar. The fractured zone and the plastic zone expand toward the center of the coal pillar, reducing the proportion of the elastic zone and redistributing the stress within the coal pillar. The stress peak and the plastic zone further expand toward the deeper regions of the coal pillar, significantly reducing its load-bearing capacity. However, due to the large width of the coal pillar, the effective load-bearing area of the coal pillar remains substantial, as shown in Figure 8(c).

3. Theoretical Analysis of Critical Coal Pillar Width

3.1 Critical Coal Pillar Width under Limit Equilibrium Theory

According to the limit equilibrium theory (Zhang et al., 2015), the stress at the boundary interface of the ultimate equilibrium zone in the coal seam is:

$$\sigma_y = \left(\frac{C_0}{\tan\varphi_0} + \frac{P_x}{l}\right) e^{\frac{2\tan\varphi_0}{Ml}} - \frac{C_0}{\tan\varphi_0} \tag{1}$$

$$\tau_{xy} = -\left(C_0 + \frac{P_x \tan\varphi_0}{l}\right) e^{\frac{2\tan\varphi_0}{Ml}x} \tag{2}$$

Width of Plastic Zone (Stress Limit Equilibrium Width):

$$R = \frac{Ml}{2\tan\varphi_0} \ln \frac{\frac{kgH}{1000} + \frac{C_0}{\tan\varphi_0}}{\frac{C_0}{\tan\varphi_0} + \frac{P_x}{l}} = \tag{3}$$

The parameters corresponding to Equation (3) are presented in Figure 2.

Table 2 Basic parameters of stress limit balance width calculation formula

Symbol	Parameter Description	Value/Unit
H	Mining depth	350 m
λ	Lateral pressure coefficient	1.05
k	Stress concentration factor	1.25
γ	Average unit weight of overlying strata	25 kN/m^3
p_x	Supporting strength of roadway support on coal rib	0.2 MPa
M	Mining thickness of coal seam	20 m
C_0	Cohesion of coal-rock interfaces (e.g., bedding planes)	2.45 MPa
φ_0	Internal friction angle of coal-rock interfaces	32.6°
-	Theoretical calculation result	Coal pillar width ≥ 21.34 m

In summary according to the limit equilibrium theory, the coal pillar width should not be less than 21.34 meters.

3.2 Critical Coal Pillar Width under Strength Theory

For strip coal pillars, where the length L is much greater than the width a, they are regarded as a plane problem, ignoring the edge effects at the front and rear ends of the strip coal pillar. Under this condition, the ultimate load that the coal pillar can bear is given a (Wang et al., 2002):

$$\sigma_s = \left(\frac{2C\cos\varphi}{1-\sin\varphi} + \frac{1+\sin\varphi}{1-\sin\varphi} k\gamma H\right) \times \left(a - 0.00492\lambda MH\right) L \tag{4}$$

Actual load bearing of the coal pillar:

$$\sigma_p = \gamma H \left[a + \frac{b}{2}\left(2 - \frac{b}{0.6H}\right)\right] L \tag{5}$$

The parameters corresponding to Equation (5) are presented in Figure 3.

Table 3 The basic parameters of the actual bearing formula of coal pillar

Symbol	Parameter Description	Value/Unit
b	Mining width (dip width of the working face)	244.6 m
C	Cohesion of the coal body	2.45 MPa
φ	Internal friction angle of the coal body	32.6°
k	Stress concentration factor	1.25
L	Length of the coal pillar	1500 m

The necessary condition to ensure the coal pillar remained stable is:

$$\sigma_p \le \sigma_s \tag{6}$$

By combining Equations (4), (5), and (6), the coal pillar width is determined to satisfy the following condition (Wang et al., 2002):

$$a \ge \frac{\frac{\gamma H\left(1.2bH - b^2\right)}{4.8H} + 0.00123\lambda MH \frac{2C\cos\varphi + k\gamma H\left(1+\sin\varphi\right)}{1-\sin\varphi}}{\frac{2C\cos\varphi}{1-\sin\varphi} + \frac{1+\sin\varphi}{1-\sin\varphi} k\gamma H - \gamma H} \tag{7}$$

From Equation (7), it is determined that when the coal pillar width exceeds 26.18 m, the actual load borne by the coal pillar does not exceed the ultimate load, and the coal pillar remains stable. Therefore, under the strength theory, the coal pillar width should not be less than 26.18 m.

Combining the theoretical analysis results from Sections 3.1 and 3.2, the critical width of the protective coal pillar for the recovery roadway in the First Panel at the Suancigou Coal Mine is determined as max(21.34, 26.18) = 24.45 m. Thus, the minimum coal pillar width should not be less than 26.18 m.

4. Analysis of Governance Effectiveness

4.1 Model Construction and Simulation Scheme

Based on the engineering geological parameters of the Suancigou Coal Mine, a two-dimensional calculation model is established using Phase 2. The model dimensions are 644 m × 200 m, as shown in Figure 9. The bottom boundary of the model is fixed, the top boundary is free, and horizontal displacement constraints are applied to all other boundaries. The weight of the overlying strata above the model is applied to the upper boundary in the form of a uniformly distributed load, with a magnitude of 6.88 MPa. The Mohr-Coulomb constitutive model is selected for the material of the model elements.

Due to the large thickness of the coal seam, local large deformations of the mesh might cause errors during the calculation. To address this issue, flexible material parameters are assigned to the caving zone of the mined-out working face to ensure accuracy and convergence during the model calculation (Wang et al., 2025; Sebacher and Hanea, 2024; Shi et al., 2024).

Based on the theoretical calculation results in Chapter 3, the simulation scheme is designed to perform calculations for coal pillar widths of 35 m, 30 m, and 25 m. According to actual working conditions, the roadway dimensions are set to 5.4 m (width) × 3.8 m (height). The simulation calculations are divided into three steps: roadway excavation, recovery of Working Face 1, and recovery of Working Face 2.

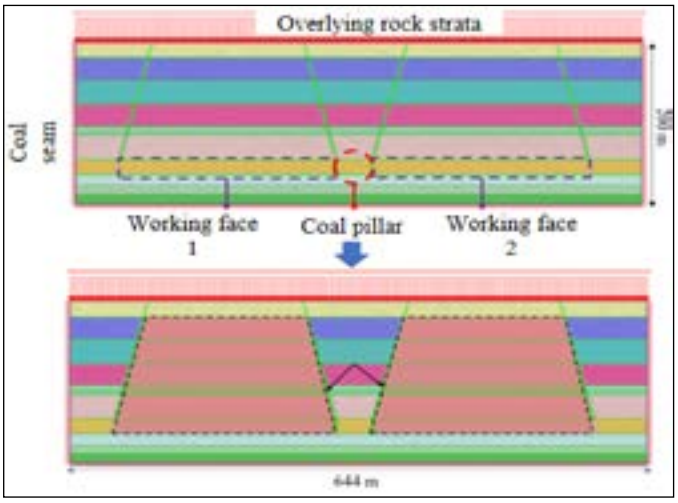

Fig.9 Model meshing diagram

4.2 Simulation Results

(1) Coal pillar width of 35 m

Figure 10 shows the stress and damage distribution characteristics of the 35 m coal pillar under the influence of mining and excavation.

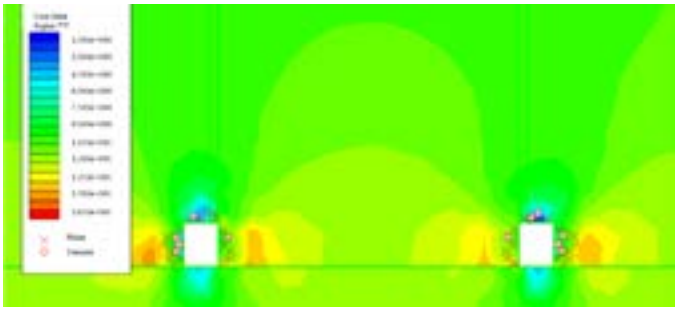

(a) Roadway Excavation

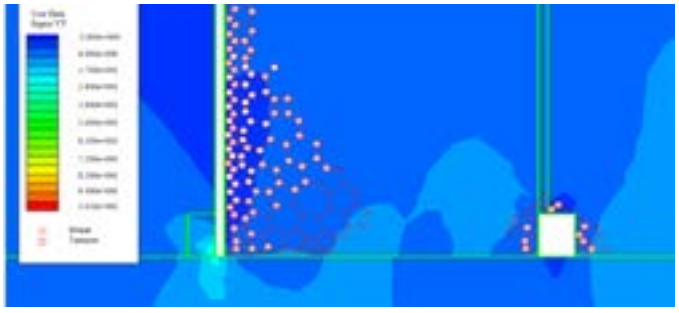

(b) Recovery of Working Face 1

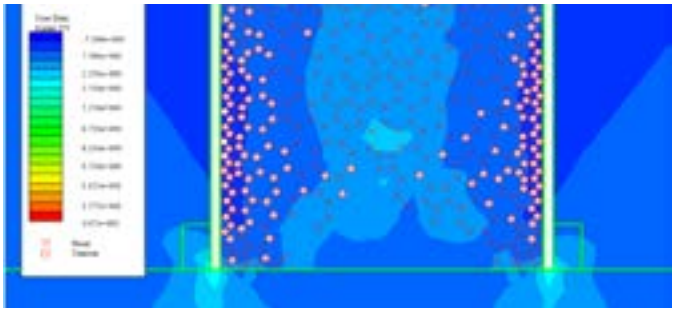

(c) Recovery of Working Face 2

Fig.10 The stress and damage distribution characteristics of the 35 m coal pillar

From Figure 10, it can be observed that during roadway excavation, the vertical stress field of the surrounding rock is symmetrically distributed around the central axis of the coal pillar. Slight stress concentration occurs near both sides of the roadway, and there is some damage and failure in the shallow regions. However, due to the large width of the coal pillar, the distribution of the elastic-plastic zone within the coal pillar is not significantly affected by roadway excavation, and no notable damage is observed in the interior, as shown in Figure 10(a).

During the recovery of Working Face 1, the damaged area on the side of the coal pillar near the goaf gradually expands toward the interior of the coal pillar, and the plastic zone begins to develop. A slight stress concentration phenomenon forms on the goaf side of the coal pillar. Additionally, the recovery of Working Face 1 exacerbates the shallow damage and failure of the surrounding rock in the roadway near the goaf, as shown in Figure 10(b).

During the recovery of Working Face 2, the damaged area within the coal pillar further develops toward the deeper regions of the coal pillar, forming a distinct "three-zone" distribution consisting of a fractured zone, a plastic zone, and an elastic zone, with the elastic zone accounting for the largest proportion. Furthermore, the vertical stress exhibits a symmetrical distribution along the central axis of the coal pillar, as shown in Figure 10(c).

(2) Coal pillar width of 30 m

Figure 11 shows the stress and damage distribution characteristics of the 30 m coal pillar under the influence of mining and excavation.

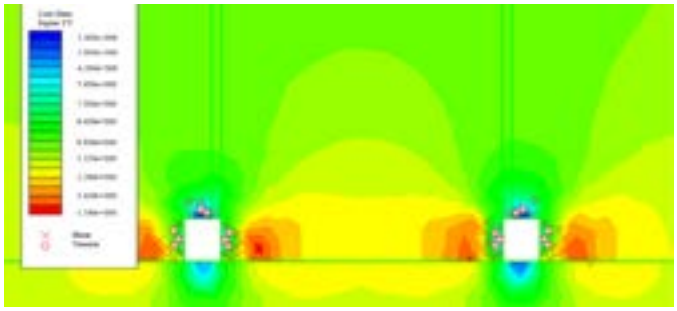

(a) Roadway Excavation

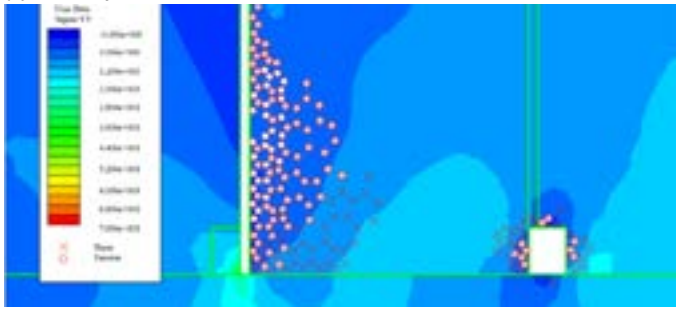

(b) Recovery of Working Face 1

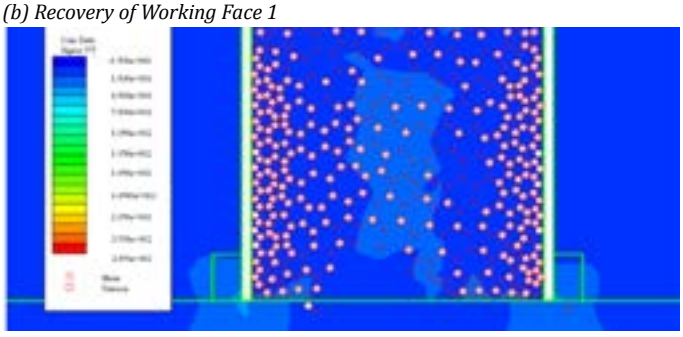

(c) Recovery of Working Face 2

Fig.11 The stress and damage distribution characteristics of the 30 m coal pillar

From Figure 11, it can be observed that during roadway excavation, the vertical stress field within the coal pillar exhibits an approximately "saddle-shaped" pattern, symmetrically distributed along the central axis of the coal pillar. The maximum vertical stress is 16.2 MPa, as shown in Figure 11(a).

During the recovery of Working Face 1, similar to the 30 m coal pillar, the plastic zone of the coal pillar continuously expands toward its interior, and the fractured zone gradually begins to develop and expand. The vertical stress exhibits an asymmetric distribution pattern. Likewise, the recovery of Working Face 1 exacerbates the damage and failure of the surrounding rock in the roadway near the goaf, as shown in Figure 11(b).

During the recovery of Working Face 2, the damaged and fractured zones within the coal pillar gradually connect, causing large-scale failure of the coal pillar and a significant reduction in its load-bearing capacity, as shown in Figure 11(c).

(3) Coal pillar width of 25 m

Figure 12 shows the stress and damage distribution characteristics of the 25 m coal pillar under the influence of mining and excavation.

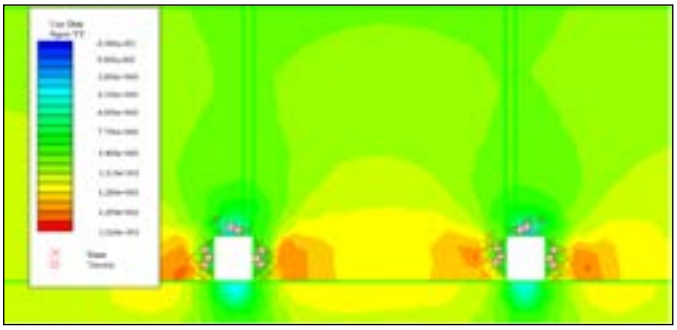

(a) Roadway Excavation

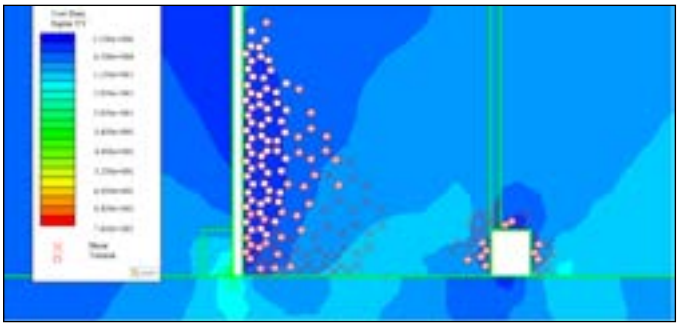

(b) Recovery of Working Face 1

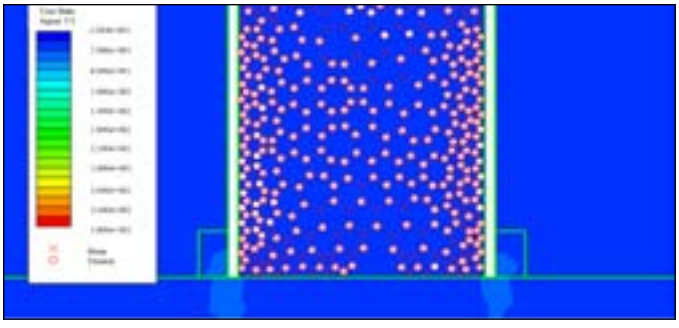

(c) Recovery of Working Face 2

Fig.12 The stress and damage distribution characteristics of the 25 m coal pillar

From Figure 12, it can be observed that during roadway excavation, the vertical stress field is symmetrically distributed along the central axis of the coal pillar. The maximum vertical stress is 15.6 MPa, and the overlapping stress region increases, resulting in a higher degree of stress concentration, as shown in Figure 12(a).

During the recovery of Working Face 1, a plastic zone penetration phenomenon appears at the base of the coal pillar, and the fractured zone on the goaf side of the coal pillar expands and develops. Overall, the coal pillar suffers severe damage and failure. Additionally, the recovery of Working Face 1 causes the failure of the surrounding rock in the exposed roadway to extend deeper, significantly reducing its stability, as shown in Figure 12(b).

During the recovery of Working Face 2, the fractured zone of the coal pillar becomes completely penetrated, leading to the overall failure of the coal pillar, which loses its load-bearing capacity.

The numerical calculation results indicate that the coal pillar width should not be less than 25 m and not exceed 30 m. Multiple mining and excavation activities have a severe impact on the stress distribution, the degree of fracturing, and the load-bearing capacity of coal pillars with widths between 25 m and 30 m. However, after the recovery of Working Face 1, the coal pillar still retains a significant load-bearing capacity, and certain technical measures can be applied to control the stability of the exposed roadway to ensure the safe recovery of Working Face 2.

Therefore, it is concluded that the coal pillar width for the 6_{upper} coal seam in the Suancigou Coal Mine should not be less than 25 m and not exceed 30 m. This range ensures a high coal recovery rate while guaranteeing the safe recovery of the working face. However, due to the significant variations in coal seam thickness, it is necessary to adopt roadway reinforcement support measures in areas with greater coal seam thickness.

5. Conclusions

(1) Under the influence of multiple mining and excavation activities, the 45-meter-wide protective coal pillar still retains a significant elastic zone and maintains a high load-bearing capacity. Therefore, the original coal pillar width can be reduced to a certain extent to improve the coal recovery rate of the mine.

(2) Theoretical calculations determined that the minimum critical width of the protective coal pillar is 26.18 m, meaning the coal pillar width should not be less than 26.18 m.

(3) When the coal pillar width is no less than 25 m and no more than 30 m, it achieves a high coal recovery rate, ensures the economic benefits of the mine, and guarantees safe mining operations. However, due to significant variations in coal seam thickness, roadway reinforcement support measures must be adopted in areas with greater coal seam thickness.

Acknowledgements

This work was supported by the National Natural Science Foundation of China (52204127) and the Chongqing Scientist Responsibility System Project (Grant No. CSTC2022YCJH-BGZXM0005). The authors gratefully acknowledge the financial support from the organizations.

Author Contributions

Yongwei Du developed the computational model and performed the simulations. Zhongqiu Wang analyzed the data and interpreted the results. Xueqi Zhang and Hongbin Li prepared the manuscript with contributions from all co-authors.

Conflict of Interest

The authors declare no conflicts of interest.

Informed Consent

Informed consent was obtained from all participants involved in the study.

Reference

Cao, J., & Wei, X. 2024. Research on mining-induced surface soil cracking mechanism and development depth of downward fracture. *Engineering Failure Analysis*, 160, 108180. https://doi.org/10.1016/j.engfailanal.2024.108180

Chang, H.W., Xu, Q.Y. 2021. Determination of Coal Pillar Width of Gob-side Entry Driving with Fully Mechanized in Medium-thick Coal Seam. *Coal Technology*, 40(10), 27-31. DOI: 10.13301/j.cnki.ct.2021.10.007

Chen, F., Yu, H., Bian, Z., & Yin, D. 2021. How to handle the crisis of coal industry in China under the vision of carbon neutrality. *Journal of China Coal Society*, 46(06), 1808-1820.

Chen, S.J. 2005. Test Study of Coal's Strength & Deformation Characterestic and Application in Strip Pillar Design (in Chinese). Shandong University of Science and Technology.

Gao, L., Liu, P.Z., Zhang, P.D., Wu, G.Y., Kang, X.T. 2022. Influence of fracture types of main roof on the stability of surrounding rock of the gob-side coal-rock roadway in inclined coal seams and its engineering application. *Coal Geology & Exploration*, 50(06), 73-80. DOI: 10.12363/issn.1001-1986.21.10.0588

Gu, W., Xu, D., Wang, Y., Miao, K., Yao, S., Zhang, H., & Han, Z. 2024. Research on the stability and water isolation of waterproof coal pillars between adjacent working faces under the influence of water ponding goaf—a case study. *Applied Sciences*, 14(2), 884. https://doi.org/10.3390/app14020884

Guo, L.Q., Cai, Q.P., Peng, X.Q. 2014. Effect of strength criterion on design of strip coal pillar. *Rock and Soil Mechanics*, 35(03), 777-782. DOI: 10.16285/j.rsm.2014.03.024

He, F., Zhai, W., Song, J., Xu, X., Wang, D., & Wu, Y. 2023. Reasonable coal pillar width and surrounding rock control of gob-side entry driving in inclined short-distance coal seams. *Applied Sciences*, 13(11), 6578. https://doi.org/10.3390/app13116578

Kong, F.L., Liu, J.D., Tian, L.T., Zhang, Z.Q., Wang, D.D., Zheng, Z.Q., Xu, Q. 2022. Study on reasonable width of coal pillar under water-rock interaction. *Journal of Mine Automation*, 48(12), 144-150. DOI: 10.13272/j.issn.1671-251x.2022060062

Li, L., Bo, J.B., Wang, X.Y. 2012. Rational position and control technique of roadway driving along next goaf in fully mechanized top coal caving face. *Journal of China Coal Society*, 37(09), 1564-1569. DOI: 10.13225/j.cnki.jccs.2012.09.029

Li, X., Li, H., Zhang, X., Yuan, H., Li, X., Shi, C., Lei, G. 2024. Damage evolution of coal with a strong bursting liability and 3d measurement method for elastic deformation energy distribution. *Theoretical and Applied Fracture Mechanics*, 133(Part A), 104534. https://doi.org/10.1016/j.tafmec.2024.104534

Li, Z., Fan, J., Feng, G., Qi, C., & Zhang, J. 2023. A new method for identifying coal pillar instability based on energy and stress correlation characteristics and its engineering application. *Minerals*, 13(12), 1507. https://doi.org/10.3390/min13121507

Liu, B., Zhu, L., Liu, X., Liu, Q., Fan, Y., Yao, W., & Deng, W. 2024. Energy evolution and damage deformation behavior of cemented broken coal specimen under triaxial compression condition. *Energy*, 310, 133203. https://doi.org/10.1016/j.energy.2024.133203

Liu, Q., Xue, Y., Ma, D., & Li, Q. 2023. Failure characteristics of the water-resisting coal pillar under stress-seepage coupling and determination of reasonable coal pillar width. *Water*, 15(5), 1002. https://doi.org/10.3390/w15051002

Rong, Y., Sun, Y., Chen, X., Ding, H., & Xu, C. 2024. Analysis of damage and permeability evolution of sandstone under compression deformation. *Applied Sciences*, 14(16), 7368. https://doi.org/10.3390/app14167368

Sebacher, B., & Hanea, R. 2024. Bridging element-free galerkin and pluri-gaussian simulation for geological uncertainty estimation in an ensemble smoother data assimilation framework. *Petroleum Science*, 21(3), 1683-1698. https://doi.org/10.1016/j.petsci.2023.12.020

Shi, H., Li, J., Shen, H., Li, X., Wei, N., Wang, Y., Pan, H. 2024. Quantitative analysis of the numerical simulation uncertainties from geological models in CO_2 geological storage: a case study of shenhua CCS project. *International Journal of Greenhouse Gas Control*, 135, 104142. https://doi.org/10.1016/j.ijggc.2024.104142

Song, H. 2016. The Current Status and Development Trends of Strip Mining Research in China (in Chinese). *Technology and Market*, 23(08), 197-198.

Tian, J.S., Jia, J.D., Zhu, H.Y., Lian, K.Y. 2021. Reasonable coal pillar width in deep high-stress working face with double lane. *Coal Engineering*, 53(04), 6-10.

Wang, J., Liu, Y., & Zhang, N. 2025. Advancing practical geological co_2 sequestration simulations through transfer learning integration and physics-informed networks. *Gas Science and Engineering*, 134, 205523. https://doi.org/10.1016/j.jgsce.2024.205523

Wang, X.C., Huang, F.C., Zhang, H.X., Zhang, L.G. 2002. Discussion and improvement for A.H.Wilsons coal pillar design. *Journal of China Coal Society*, (06), 604-608.

Wang, X.Y., Dou, S.Y. 2022. Determination of small coal pillar parameters in goaf excavation of fully-mechanized caving face in Tongxin Coal Mine. *Coal Science - Technology Magazine*, 43(06), 44-48+52. DOI: 10.19896/j.cnki.mtkj.2022.06.011

Xie, H., Ren, S., Xie, Y., & Jiao, X. 2021. Development opportunities of the coal industry towards the goal of carbon neutrality. *Journal of China Coal Society*, 46(07), 2197-2211.

Xing, K., Cheng, J., Zhen, Z., Wan, Z., Han, Z., Yan, W., Yang, Y. 2024. Effect of super-high water materials backfilling on stress decrease and energy release during strip coal pillar mining: a case study. *Heliyon*, 10(18), e37441. DOI: 10.1016/j.heliyon.2024.e37441

Xue, Y.P. 2024. Optimization of small coal pillar width and control measures in gob-side entry excavation of thick coal seams. *Scientific Reports*, 14(1), 23304. https://doi.org/10.1038/s41598-024-74793-8

Yang, T., Zhang, Y., Zhang, J., Lin, H., Bao, R., He, Y., Pang, H. 2024. Study on the stability and reasonable width of coal pillars in "three soft" coal seams based on a physical similarity simulation experiment. *Applied Sciences*, 14(14), 6127. https://doi.org/10.3390/app14146127

Yang, Y., Li, Y., Wang, L., & Wu, Y. 2023. On strata damage and stress disturbance induced by coal mining based on physical similarity simulation experiments. *Scientific Reports*, 13(1), 15458. https://doi.org/10.1038/s41598-023-42148-4

Yang, Y., Sun, J., Wang, W., & Zhang, R. 2022. Research on coal pillar width and support design of gob-side entry. *Geotechnical and Geological Engineering*, 41(2), 847-860. https://doi.org/10.1007/s10706-022-02309-0

Yin, S.F., Zuo, A.J., Ma, L.J., Ren, Y.X., Shi, S.H. 2022. Surrounding rock stability during gob-side entry driving with narrow coal pillar in medium-thick coal seam. *Coal Engineering*, 54(05), 90-96.

Yuan, L., Wang, E., Ma, Y., Liu, Y., & Li, X. 2023. Research progress of coal and rock dynamic disasters and scientific and technological problems in China. *Journal of China Coal Society*, 48(05), 1825-1845. DOI: 10.13225/j.cnki.jccs.2023.0264

Yun, Q.L., Wang, X.H., Jing, W., Zhang, W.B., Wei, X.X., & Wang, J.H. 2024. Characteristics of deformation and damage of surrounding rock along the top roadway in the working face of an isolated island and its evolution law. *Scientific Reports*, 14(1), 15092. https://doi.org/10.1038/s41598-024-63246-x

Zhang, K.X., Zhang, Y.J., Ma, Z.Q., Bi, W.G., Yang, Y.M., Li, Y. 2015. Determination of the narrow pillar width of gob-side entry driving. *Journal of Mining and Safety Engineering*, 32(03), 446-452. DOI: 10.13545/j.cnki.jmse.2015.03.016

Zheng, Z., Yang, Z.Q., Zhu, H.Z., He, F.L., Du, C.Y., Liu, B.Q. 2019. Study on reasonable coal-pillar width and surrounding-rock control of gob-side irregular roadway in inclined seam. *Journal of Mining and Safety Engineering*, 36(02), 223-231. DOI: 10.13545/j.cnki.jmse.2019.02.002

Zhu, S.T., Wang, B., Jiang, F.X., Zhang, X.F., Sun, X.K., Sun, X., Liu, J.H., Zhang, A.M. 2021. Study on reasonable width of isolated coal pillar based on rock burst-mine earthquake coordinated control. *Coal Science and Technology*, 49(06), 102-110. DOI: 10.13199/j.cnki.cst.2021.06.012